Indian Journal of Biochemistry & Biophysics
Vol. 63, August 2026, pp. 958-968
DOI: 10.56042/ijbb.v63i8.20784

Simulated docking and binding of Conantokin-P and Conantokin-Pr3 to NMDA receptor GluN2B subunit: Roles of calcium ions and gamma-carboxyglutamate residues

Aaron Noel Parong Genato[1], Stephen Kyle Cordero Arcan[2,4], Elsie Candelaria Jimenez[3] & Neil Andrew David Bascos[2,4]*

[1]Department of Physical Sciences and Mathematics, College of Arts and Sciences, University of the Philippines Manila, Padre Faura St., Manila, Philippines

[2]Protein, Proteomics, and Metabolomics Facility, Philippine Genome Center, University of the Philippines System

[3]Department of Physical Sciences, College of Science, University of the Philippines Baguio, Baguio City 2600, Philippines

[4]Protein Structure and Immunology Laboratory, National Institute of Molecular Biology and Biotechnology, University of the Philippines Diliman, Quezon City 1101, Philippines

Received 18 June 2025; *revised 16 March 2026*

Conantokin-P (con-P) and conantokin-Pr3 (con-Pr3), peptides isolated from *Conus* venoms have shown high potency and selectivity for the N-methyl-D-aspartate (NMDA) receptor GluN2B subunit. In this work, structural bases for these characteristics were investigated through *in silico* modelling and molecular dynamics simulations. Con-P and con-Pr3 were predicted to adopt stable α-helical conformations in the presence of Ca^{2+}. The non-standard gamma-carboxyglutamate (Gla) residues in these conotoxins were observed to be important for the association of Ca^{2+}. In con-P and con-Pr3, Gla residues form salt bridges with GluN2B basic amino acid residues. Additionally, basic amino acid residues of the conantokins form salt bridges with GluN2B acidic residues. Calcium binding is shown to enhance the participation of Gla residues in salt-bridge formation of both con-P and con-Pr3. Molecular docking revealed the existence of con-P binding sites in both the external and internal faces of the GluN2B amino-terminal domain–agonist-binding domain (ATD-ABD) pocket. In contrast, con-Pr3 docked only to the internal face. For con-P, increased hydrogen bond interactions and more salt bridges were observed for docks at the external face compared to those at the internal face. Additionally, con-P binding at the external face of the ATD-ABD pocket can induce an inward stretching motion for the ATD. This stretching occurred with greater magnitude in the presence of Ca^{2+}, suggesting that Ca^{2+} influenced conformational changes in the external face of the ATD-ABD pocket. Calcium ions also cause outward stretching for con-P, when bound at the internal face of the ATD-ABD pocket. Interestingly, for con-Pr3, Ca^{2+} resulted in minimal movement, while large outward stretching was observed in Ca^{2+}-free conditions. Notably, the observed binding affinities for con-Pr3 reflect similar magnitudes as previous studies. Furthermore, molecular dynamic simulations revealed that con-P may form both dimers and trimers that are sustained by multiple Ca^{2+}-Gla intermolecular bridges, while con-Pr3 may entail the recruitment of three sets of Gla residues to form a stable multimer. These characterizations of conotoxin binding to NMDA receptors provide bases for the development and testing of conantokin-based therapies for neurological conditions.

Keywords: Conantokin, Conotoxin/conopeptide dimers and trimers, *Conus* venom, GluN1, GluN2A, GluN2B, N-methyl-D-aspartate receptor

The N-methyl-D-aspartate (NMDA) receptors are ligand-gated cation channels that have vital roles in the development of the central nervous system (CNS). They have different subunits, and their variants have various functions in the brain. These tetrameric NMDA receptors are either of the diheteromeric, or the triheteromeric subtype. Diheteromeric NMDA receptors are made up of two GluN1 subunits and two identical GluN2 subunits. Triheteromeric NMDA receptors are composed of two GluN1 subunits and two different GluN2 subunits (e.g., GluN2A and Glu N2B). The GluN1/GluN2A/GluN2B (also referred to as NR1/NR2A/NR2B) triheteromeric subtype is posited to be the most abundant in the adult forebrain[1,2].

Because of their role in the CNS, the NMDA receptors are considered as prime drug targets for various neurological disorders. Cognitive symptoms linked to deficits in learning and memory, such as in Alzheimer's disease, have been associated with disorders in glutaminergic neurotransmission. Excessive stimulation of neurons by the glutamate neurotransmitter

*Correspondence:
E-mail: ndbascos@up.edu.ph
Suppl. data available on respective page of NOPR

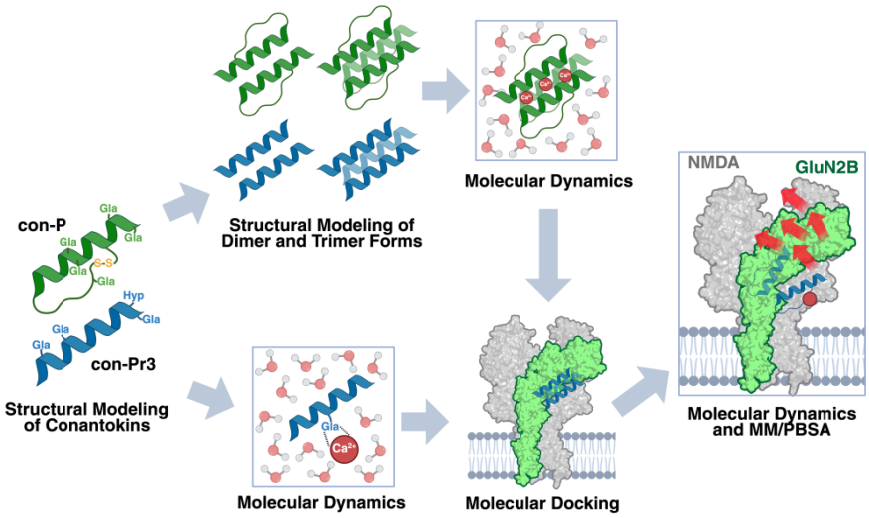

Graphical abstract

Table 1 — Conantokin sequences and preferred target NMDAR subtypes

Conantokin	Amino acid sequence	NMDAR subunit	*Conus* species	Reference
Con-G	GEUULQUNQU LIRUKSN*	GluN2B	*C. geographus*	26,27
Con-T	GEUUYQKMLU NLRUAEVKKN A*	GluN2B	*C. tulipa*	28,29
Con-R	GEUUVAKMAA ULARUNIAKG CKVNCYP	GluN2B	*C. radiatus*	30
Con-Pr1	GEDUYAUGIR UYQLIHGKI	GluN2B	*C. parius*	9
Con-Pr2	DEOUYAXAIR UYQLKYGKI	GluN2B	*C. parius*	9
Con-Pr3	GEOUVAKWAU GLRUKASSN*	GluN2B	*C. parius*	9
Con-P	GEUUHSKYQU CLRUIRVNKV QQUC*	GluN2B	*C. purpurascens*	8
Con-Br	GDUUYSKFIU RERUAGRLDL SKFP	GluN2B	*C. sulcatus*	31
Con R1-B	GEUULAUKAO UFARULAN*	GluN2B	*C. rolani*	32
Con Bk-A	GDUUYSUFIU RERULVSSKI PR	GluN2D	*C. bocki*	33
Con Bk-B	GDUUYSUAI*	GluN2D	*C. bocki*	33
Con Bk-C	DDUUYAUFIU QQRUAGLV	GluN2D	*C. bocki*	33

NMDAR, N-methyl-D-aspartate receptor; U, gamma-carboxyglutamate; O, 4-*trans*-hydroxyproline; C*, amidated C-terminus. GluN2A, GluN2B and GluN2D are also referred to as NR2A, NR2B and NR2D, respectively.

leads to excitotoxicity resulting in neuron damage and death[3]. Hence, inhibiting the glutaminergic neurotransmission by NMDA receptors can ease the excitotoxicity and prevent damage and death of neurons.

The conantokins comprise a family of cone snail (genus *Conus*) venom peptides that are NMDA receptor antagonists. Several conantokins have defined target NMDA receptor subtypes (Table 1). Unlike other *Conus* toxins, most conantokins lack disulfide linkages. Instead, conantokins contain multiple residues of gamma-carboxyglutamate (Gla), a post-translationally modified amino acid. The Gla residues usually confer a helical structure to conantokins by coordinating divalent metal ions[4].

Beyond the stabilization of their helical structures, conantokins rely on a metallozipper motif, allowing Ca^{2+} to mediate intermolecular bridging between Gla residue without the need for a hydrophobic interface[5]. Here, Ca^{2+} acts as an electrostatic bridge that neutralizes the dense negative charges of the Gla side chains, allowing peptide backbones to associate. Previous reports on the crystal structures of calcium-bound conantokin-G (con-G) and con-T[K7Gla] variants demonstrated an antiparallel dimerization induced by Ca^{2+}. While their metal-chelation sites are similar, the dimer interfaces of con-G and con-T[K7Gla] are structurally distinct, presenting a unique structural basis of the helix association[5,6]. Additionally, mutations alter steric hindrances and coordination geometry thereby affecting oligomerization. Such mutations like con-G[Q6A] replace the bulky side chain of glutamine with smaller alanine, facilitating the formation of a metal-dependent helix trimerization[7]. The Ca^{2+} chelation across the helix interfaces dominates such parallel/antiparallel trimeric helix bundle, which allows further stabilization of

monomeric, dimeric, and even trimeric metallozippers based on their sequence and cation availability[7].

The conantokin-P (con-P), characterized in *Conus purpurascens* venom ducts, is different from other members of the conantokin family. Con-P, which consists of 24 amino acid residues, is less helical than the other previously characterized conantokins based on circular dichroism. Con-P has five Gla residues and a long disulfide loop consisting of 12 amino acids. Two Gla residues are placed between the Cys residues in this loop. Con-P blocks the NMDA receptor GluN2B with submicromolar potency[8].

The conantokin-Pr3 (con-Pr3), isolated from *Conus parius* venom, consists of 19 amino acids including three Gla residues. It contains several amino acids that differ from earlier known conantokin consensus sequences. Con-Pr3 notably lacks Gla at the 3rd position from the N-terminus. This Gla residue is substituted by 4-*trans*-hydroxyproline (Hyp), another post-translationally modified amino acid. Unlike other conantokins, Con-Pr3 adopts an alpha-helical conformation even in the absence of divalent cations. Like the other conantokins, it elicits sleep in young mice and hyperactivity in older mice upon intracranial injection. Electrophysiological assays confirm that con-Pr3 is an NMDA receptor antagonist, with approximately 10-fold selectivity for the NMDA receptor GluN2B[9].

The studies on con-P and con-Pr3 indicate that different *Conus* species evolve to produce diverse groups of conantokins with unique biochemical and structural features. Some of these features may converge to increase specificity for similar targets. Investigating these distinct features in con-P and con-Pr3 allows the definition of structural bases through which conantokins selectively target NMDA receptors.

In silico experiments were performed to characterize the structural features and predicted interactions of con-P and con-Pr3 with their target NMDA receptor, specifically the GluN2B subunit. The results provide structural bases for the preferential binding of specific conantokin features to select target surfaces. This information supports the development of conantokin-based pharmacological agents for the treatment of neurological disorders.

Materials and Methods

Structure preparation

The sequence and structural features of con-P were based on the characterization by Gowd and colleagues[8]. The unmodified peptide was modeled using the C-I-TASSER server (http://zhanglab.ccmb.med.umich.edu), which allowed the prediction of a disulfide-loop structure by specification of residue contact between Cys11 and Cys24[10]. The Gla residue and amidated C-terminus were modeled in CHARMM-GUI[11].

The sequence and structural features of con-Pr3 were based on the characterization by Teichert and colleagues[9]. Its unmodified peptide sequence was modeled with the I-TASSER server[12]. The Gla and Hyp residues, and amidated C-terminus were added using the CHARMM-GUI PDB reader.

To model the potential dimeric and trimeric forms, X-ray crystal structures of the antiparallel dimeric conantokin-G (con-G)(PDB ID: 2DPQ) and conantokin-T(K7Gla)(PDB ID: 2DPR)[5]; and trimeric con-G(Q6A)(CCDC 683228)[7] served as templates where con-P and con-Pr3 representative structures were aligned.

To model the NMDA receptor, the PDB structure of the human GluN1/GluN2A NMDA receptor in the glutamate/glycine-bound state (PDB ID: 6IRA) was used as a reference structure[13]. Sequences of human GluN1, GluN2A, and GluN2B subunits were obtained from UniProt and were submitted to I-TASSER with PDB:6IRA as template to generate the complete subunit structures. The generated structure has a high similarity to an available structure in the Alphafold Protein Data Bank, with an RMSD of 4.735 A (Suppl. Fig. 1). Tetrameric structures for the GluN1/GluN2A; GluN1/GluN2A/GluN2B; and GluN1/GluN2B were assembled using the align function in PyMOL[14].

Molecular dynamics parameters

Molecular dynamics (MD) simulations were performed using the GROMACS suite 2023.2[15]. The CHARMM36 all-atom force field was chosen for the availability of parameters for the non-standard amino acids, Gla and Hyp[16]. All systems consisted of a cubic unit cell with a protein-box distance of 1.0 nm solvated with TIP3P water and neutralized with either Na^+ or Ca^{2+}, and Cl^- to a concentration of 0.01 M.

Energy minimization was conducted using the steepest descent algorithm until the maximum force was less than 1000.0 kJ mol^{-1} nm^{-1}. The system was then first equilibrated by isothermal-isochoric equilibration for 100 ps, followed by isothermal-isobaric equilibration for 100 ps at 1 bar with the Parrinello-Rahman barostat. Temperature was maintained at 300 K for both steps. Production MD

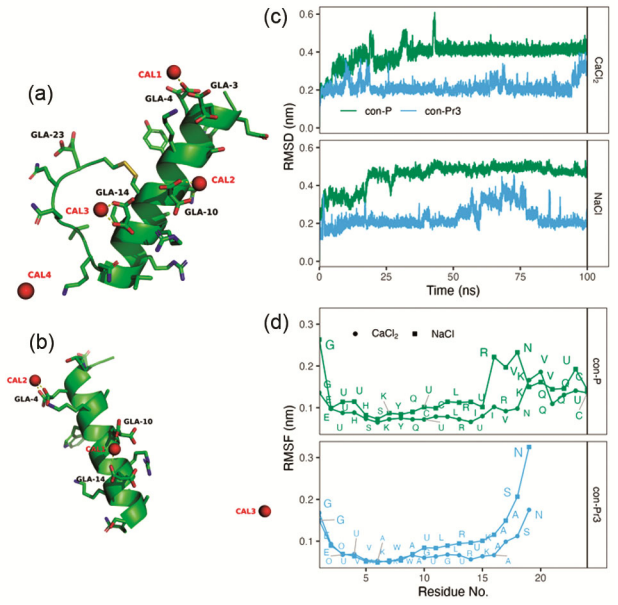

Fig. 1 — Stabilization of con-P and con-Pr3 by Ca^{2+} ions. Representative structures of con-P (a) and con-Pr3; (b) bound to Ca^{2+} ions, showing minimum distance of each Ca^{2+} ion (Con-P: CAL1, CAL2, CAL3, & CAL4; Con-Pr3: CAL1, CAL2, & CAL3) from con-P and con-Pr3 during production MD in 0.01M $CaCl_2$; (c) Total protein RMSD of individual conantokins in 0.01M $CaCl_2$ or NaCl; and (d) Per-residue RMSF of individual conantokins solvated in 0.01M $CaCl_2$ or NaCl

was performed with 2 fs time step with applied periodic boundary conditions. Con-P and con-Pr3 were run for 100 ns while the complete NMDA GluN1/GluN2A/GluN2B receptor was run for 1 ns. Conantokin:NMDA complexes were run for 5 ns.

Analyses of production MD trajectories were done with the GROMACS suite to determine whole protein RMSD, per-residue root-mean-square fluctuation (RMSF), define secondary structure of proteins (DSSP), hydrogen bond count. The Visual Molecular Dynamics (VMD) Salt Bridges tool was used to determine salt-bridge interactions [17].

Molecular dynamics simulation: Modelling the monomeric, dimeric, and trimeric forms of conantokins

The representative structures for con-P and con-Pr3 were obtained from the MD trajectories using the GROMACS suite's gmx cluster function using the single linkage method with a root-mean-square deviation (RMSD) cutoff of 0.1 nm.

The representative structures for the conantokin dimers and trimers were identified using a dimensionality reduction and Free Energy Landscape (FEL) analysis[18]. Principal Component Analysis (PCA) was performed on the alpha-carbon atom fluctuations to identify the primary collective variables of the system. The trajectory was projected onto the first two principal components (PC1 and PC2), and the joint probability distribution was used to construct a Free Energy Landscape via the relationship $G = -k_B T \ln(P(PC1,PC2))$. The representative structure was defined as the configuration corresponding to the global free energy minimum (the most populated state) on the FEL. All statistical analyses and landscape mapping were conducted in GROMACS and R.

Molecular docking: Conantokins to NMDA GluN1/GluN2A/GluN2B

Conantokins were docked to the NMDA GluN1/GluN2A/GluN2B extracellular domain tetramer using the ClusPro 2.0 docking server[19]. The choice of the extracellular domain was to avoid docks associated with the transmembrane domain of the NMDA receptor. The representative PDB structures of conantokins were submitted without post-translational modifications (PTMs), except for the disulfide loop of con-P. Representative docks of sites within GluN2B were determined for each conantokin from the 'balanced' results of ClusPro 2.0.

Molecular dynamics simulation: Analysis of the conantokin:GluN2B complex

After initial docking, production MD was done on representative docks of con-P and con-Pr3 located at the internal and external pockets of the glutamate-binding domain with PTMs included. To account for the effect of bound Ca^{2+} on the conformation of the conantokin and the complex, production MD was performed both with pre-bound Ca^{2+} (Ca^{2+}-bound), and 'Ca^{2+}-free' states in 0.01 M $CaCl_2$. Given that the dock outputs from ClusPro 2.0 do not contain PTMs, the representative PTM-containing structures of the conantokins were aligned to their docked counterparts in PyMOL, prior to the MD simulations.

Binding energy estimation

Analysis of binding energy by Molecular Mechanics Poisson-Boltzmann Surface Area (MMPBSA) was done using the gmx_MMPBSA tool[20]. The binding energy $\Delta G_{binding}$ was calculated by the following equation:

$$\Delta G_{binding} = \Delta G_{complex} - (\Delta G_{receptor} - \Delta G_{ligand})$$

Where $\Delta G_{complex}$ is the total Gibbs' free energy of the complex, $\Delta G_{receptor}$ is the contributed free energy of the receptor, and ΔG_{ligand} is the contributed free energy of the ligand.

Results and Discussion

Ca^{2+}-bound conformation of con-P and con-Pr3

Stable, α-helical and Ca^{2+}-bound conformations were adopted by both con-P and con-Pr3. For con-P the helical structure was made with its long disulfide loop placed near the C-terminal end of the helix.

Calcium ions were shown to bind con-P and con-Pr3, particularly at their Gla residues. Con-P, which has more Gla residues, persistently bound three Ca^{2+} ions, while con-Pr3 bound two Ca^{2+} ions throughout the simulation run (Fig. 1A & 1B).

Calcium ion binding contributed to the stabilization of con-P as shown by stable RMSD and lower RMSF values in conditions simulating a $CaCl_2$ solution. Lower RMSF values in $CaCl_2$ were observed compared to simulations in NaCl. Variations were most pronounced in residues Arg16, Val17, and Asn18, and Ca^{2+} binding was observed to stabilize the disulfide-loop residues. Conversely, con-Pr3 stability may rely less on the presence of Ca^{2+}, as shown by the similar RMSD and RMSF values in both solvents (Fig. 1C & 1D).

Con-P and con-Pr3 binding to NMDA receptor GluN2B

Representative docks for each site in GluN2B were determined from the top-scoring docks predicted by ClusPro 2.0. Some high scoring docks were found to cluster in pockets between the amino-terminal domain (ATD) and the agonist-binding domain (ABD) (Fig. 2B, 2C, 2E & 2F). This pocket was previously determined to be the binding site for the pyrrolidinone analog PYD-106, a positive allosteric modulator of the GluN2C sub-unit[21,22]. The conantokins, however, were predicted to have two possible sites of binding to this GluN2B pocket: first, at the external face, providing more contact with the external solvent; and at the internal face, resulting in more contact with the GluN1/N2 subunits. Docks were also observed at potential allosteric sites within the ATD of GluN2B (Fig. 2A & 2D).

To further characterize these binding modes, 3Å interaction networks were mapped for both peptides at each face (Suppl. Fig. 2). These networks illustrate that both con-P (Suppl. Fig. 2A & 2B) and con-Pr3 (Suppl. Fig. 2C & 2D) utilize their gamma-carboxyglutamate (Gla) residues as primary anchors, forming dense contact clusters with basic receptor residues. This mapping confirms that the ATD-ABD pocket can sterically accommodate these helical peptides, providing a structural basis for the high docking scores observed at both the internal and external interfaces.

The predicted conantokin interactions with the internal face of the ATD-ABD pocket suggest possible access to this region of molecules larger than the known NMDA ligands (*e.g.*, PYD-106). This is supported by the fact that conantokin interactions were still predicted for this location even when docking with the full tetrameric NMDA structure in the fully closed agonist-bound state. Moreover, the accessibility of the internal face is consistent with the dynamic conformations of the full NMDA receptor from cryo-electron microscopy studies[13,23]. Within the ATD-ABD pocket, con-P docked at both the internal

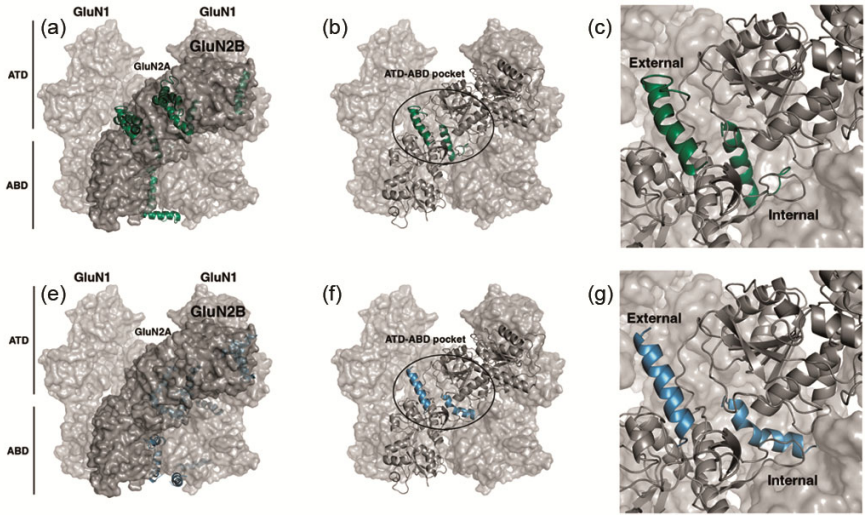

Fig. 2 — Molecular docking of con-P and con-Pr3 show binding to the ATD-ABD pocket and allosteric domains. (a) Balanced docks of con-P on GluN2B; (b) Selected high-scoring docks of con-P at the ATD-ABD pocket; (c) The ATD-ABD pocket with con-P bound at the external and internal face. (d) Balanced docks of con-Pr3 on GluN2B; (e) Selected high-scoring docks and aligned dock of con-Pr3 at the ATD-ABD pocket; (f) The ATD-ABD pocket with con-Pr3 bound at the external and internal face; and (g) The ATD-ABD pocket with con-Pr3 bound at the internal and external face.

and external faces (Fig. 2A), while con-Pr3 docked only at the internal face (Fig. 2D). To investigate the possible effect of a bound con-Pr3 at the external face, con-P docked at the external face was replaced with con-Pr3 for one simulation (Fig. 2E & 2F).

MD simulations (5 ns) of conantokin:GluN2B docks in 0.01M $CaCl_2$ suggest that con-P and con-Pr3 strongly bind to GluN2B at the external face of the ATD-ABD pocket. The structure of GluN2B remained relatively unaffected by conantokin-binding as shown by similar RMSD and RMSF values compared to the free receptor (Fig. 3A & 3B). Increased hydrogen bond interactions were observed at the external face for con-P and con-Pr3 ranging from 3 to 10 hydrogen bonds throughout the simulation. This is as opposed to the internal face with a range of 0 to 5 hydrogejsn bonds. Similarly, more salt bridge interactions were observed at the external face with up to 5 salt bridges for con-P and 4 salt bridges for con-Pr3, compared to docks in the internal face recording only a maximum of 2 salt bridges.

To investigate the effect of initial Ca^{2+} binding on docking stability and GluN2B structure, MD simulations using representative Ca^{2+}-bound conantokins were performed. In contrast to the Ca^{2+}-free simulations, disruption of GluN2B was observed in the form of increased RMSD and RMSF values (Fig. 4A & 4D). The simulations showed increased hydrogen bond and salt bridge interactions between con-P and GluN2B at the external pocket of the ATD-ABD pocket compared to Ca^{2+}-free simulations (Fig. 4B & 4C).

Conformational changes in GluN2B bound to conantokin

The induced conformational changes of GluN2B were observed based on the movement vectors of the ATD with respect to a fixed ABD. These revealed that con-P and con-Pr3 bound to the external face of the ATD-ABD pocket can induce an inward stretching motion for the ATD. A greater effect was induced by con-P (Fig. 5A & 5B). This motion has been proposed to induce a pore closing mechanism for GluN2B, which is consistent with the inhibitory effect of conantokins on NMDA receptor functions[24]. In Ca^{2+}-bound simulations, greater conformational changes are observed. Con-P stretches inward in greater magnitude compared to the Ca^{2+}-free simulation. Additionally, simulations of Ca^{2+}-bound con-P associated with the internal face of

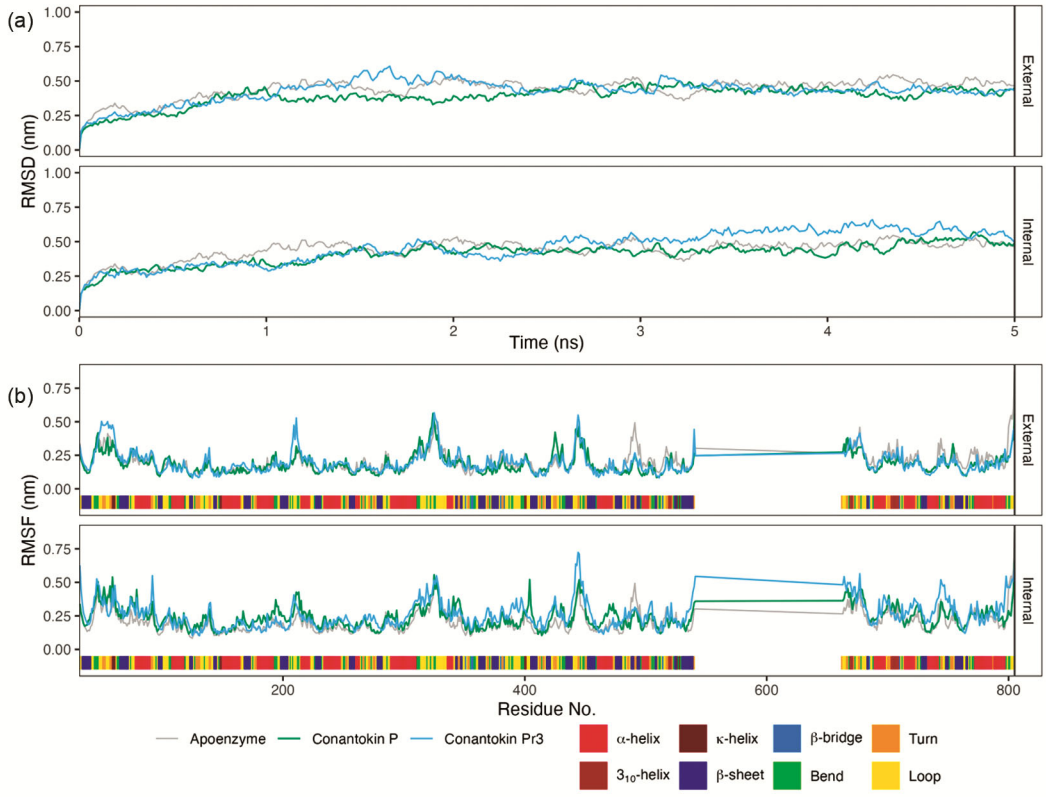

Fig. 3 — Con-P and con-Pr3 strongly associate with the external face of the ATD-ABD pocket. (a) Total protein RMSD of GluN2B; and (b) RMSF per-residue of GluN2B with endpoint secondary structure of apoenzyme

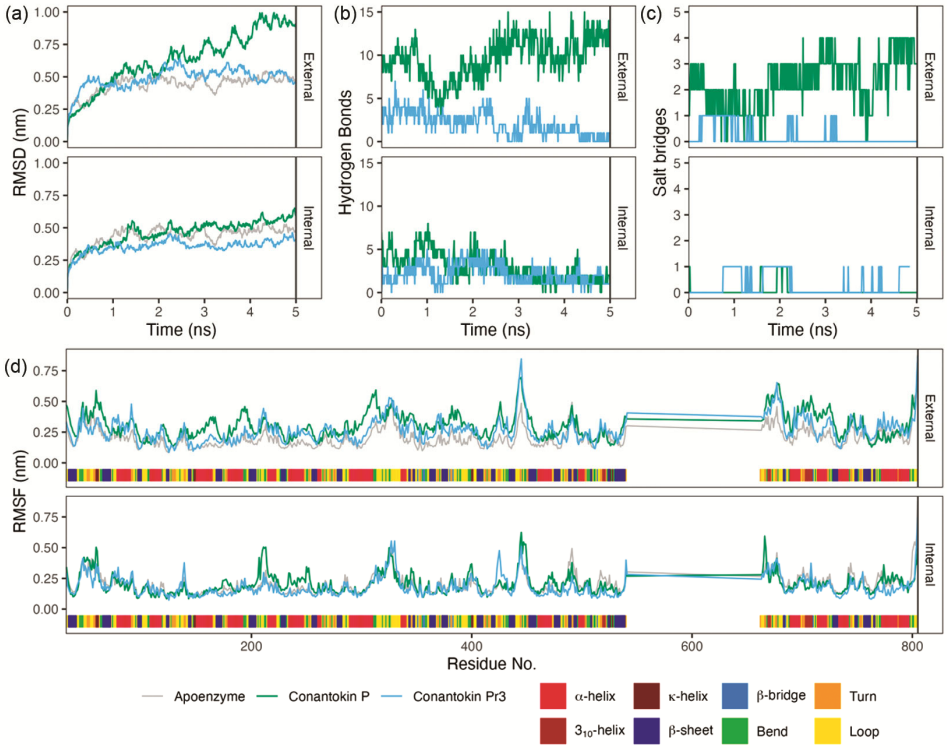

Fig. 4 — Calcium-binding to con-P enhances interactions with GluN2B. (a) Total protein RMSD of GluN2B; (b) Number of hydrogen bonds between conantokin and GluN2B; (c) Number of salt bridges between conantokin and GluN2B; and (d) RMSF per-residue of GluN2B with endpoint secondary structure of apoenzyme

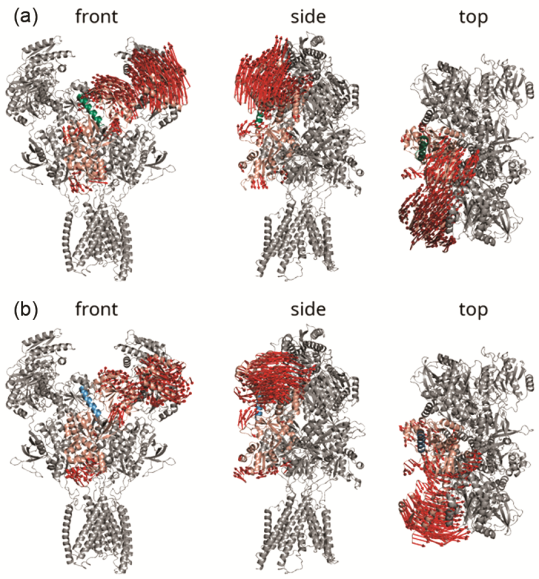

Fig. 5 — Direction of conformational changes of Ca^{2+}-free con-P (a) or con-Pr3; and (b) bound to the external face of the ATD-ABD pocket. Front, side, and top views shown

GluN2B result in large outward stretching motions for con-P. Together, these suggest that Ca^{2+} bound con-P can influence the conformational changes of the GluN2B ATD-ABD pocket.

In contrast, Ca^{2+}-free simulations with con-P bound to the internal face of the ATD-ABD pocket result only in limited conformational changes. Conversely, Ca^{2+}-free simulations predict large outward-stretching motions for con-Pr3 bound to the internal face.

Role of gamma-carboxyglutamate residues in GluN2B binding

Tracking the salt bridges formed between acidic (Gla, Glu, & Asp) and basic (Arg & Lys) residues show the involvement of the Gla residues in binding to the GluN2B ATD-ABD pocket. For con-P, Gla3 forms salt bridges with Arg439 and Arg505 while Gla23, positioned within the disulfide loop, forms salt bridges with Lys372. In con-Pr3, Gla10 forms salt bridges with Arg505. Also notable are the involvement of basic residues within the conantokin. In con-P, Arg16 and Lys19 form salt bridges with Glu397. In con-Pr3, Lys15 forms salt bridges with Glu397 and Glu400 (Table 2).

Calcium binding is shown to increase the involvement of Gla residues in salt-bridge formation. In con-P, Gla10 forms a salt bridge with Arg505 while Gla23 forms an additional salt bridge with Lys369. In con-Pr3, Gla4 forms a salt bridge with Arg393. The basic residues of con-P remain largely

Table 2 — Salt bridges formed between residues of conantokins and GluN2B

Con-P				Con-Pr3			
External		Internal		External		Internal	
Ca^{2+}-free	Ca^{2+}-bound	Ca^{2+}-free	Ca^{2+}-bound	Ca^{2+}-free	Ca^{2+}-bound	Ca^{2+}-free	Ca^{2+}-bound
E2-R439			E2-R393	E2-R439			
				E2-K438			
U3-R439	U3-R505				U4-R393		
U3-R505	U10-R505			U10-R505	U10-R505		
	U23-K369		U23-R431				
U23-K372	U23-K372						
R16-E397	R16-E400	R16-D786					
R16-D403	R16-D403	R16-E788					
K19-E397	K19-E397	R16-E791	R16-E791	K15-E397	K15-E397		
				K15-E400	K15-E397	K7-E198	K15-E191
							K15-E198

Salt bridges were detected between residues of conantokins and GluN2B throughout production MD for 5 ns. U, gamma-carboxyglutamate.

unaffected, while Lys15 of con-Pr3 loses contact with Glu400 (Table 2). The Gla3 in con-P and Gla10 in con-Pr3 were also observed to have the lowest average salt-bridge distances throughout the Ca^{2+}-bound simulation. These results are consistent with the divalent-cation dependence of con-P and suggest that con-P and con-Pr3 interactions are predominantly electrostatic.

Roles of Ca^{2+} and Gla residues in dimer and trimer structures of conantokins. The potential of the conantokins to form dimer and trimer structures was evaluated. Probable dimer and trimer structures that were generated were found to have stable RMSD values, except for dimeric con-Pr3. Notably, RMSD of the trimer structures were considerably lower than those of the dimer. This could be because more Gla residues are involved in Ca^{2+} binding. In the same vein, con-P formed stable dimer structures with the same initial conditions, likely due to it having five Gla residues in its structure. In contrast, con-Pr3, having only three Gla residues, showed higher overall RMSD and showed dimer separation during MD simulation when initially aligned to the con-T[K7Gla] dimer (Fig. 6A). However, RMSF values were consistently lower for con-Pr3 than for con-P, which may indicate a perturbation in the overall multimer, as opposed to influences by individual residues (Fig. 6B).

Structural alignment of these assemblies provides a definitive basis for these observations (Fig. 7).

For con-P at the external face, the dimers (referenced to both con-G and con-T) and the trimer show a highly ordered helical bundle. The Ca^{2+} (red spheres) are strategically positioned to bridge the Gla-rich interfaces, maintaining a tight association with the receptor. Similarly, for con-P at the internal face, the multimeric structures further exhibit more crowded internal pocket, the trimer configuration shows a robust "calcium-sandwich" that anchors the peptides effectively. In contrast, the alignment of con-Pr3 at the internal face reveals a clear reduction in structural integrity. Looking at the most represented structures, con-P shows 3 and 4 Ca^{2+} ions sandwiched between Gla residues of the dimers, and 3 Ca^{2+} ions between those of the trimer. For con-Pr3, only one dimer structure has sandwiched Ca^{2+} ions, with a disruption of the initial antiparallel conformation, and only 2 Ca^{2+} ions are shared in the trimer structure (Fig. 6C). Overall, these simulations show that con-P may form both dimers and trimers that are supported by multiple Ca^{2+}-Gla intermolecular bridges, while con-Pr3 may require the recruitment of three sets of Gla residues to form a stable multimer.

Binding energy calculation

MMPBSA calculations show con-P and con-Pr3 exhibiting “negative” binding energies, indicating stability for the interacting structures. More negative values are observed for the con-P ligand, suggesting its increased structural stability compared to con-Pr3. Greater structural stability is also observed when the conotoxins bind the external face of the ATD-ABD pocket compared to the internal face, consistent with the involvement of more hydrogen bond and salt bridge interactions. Between con-Pr3 and con-P, more negative binding energies are observed for interactions involving con-P. The presence of Ca^{2+} is observed to induce a distinct difference in binding energy for complexes with con-P bound to the internal faces of the ATD-ABD pocket. In contrast, the presence of Ca^{2+} does not result in a significant difference for the binding energies of con-Pr3 to either the external or internal faces (Table 3). These results suggest a possible Ca^{2+}-dependent effect on con-P interactions, but not for con-Pr3.

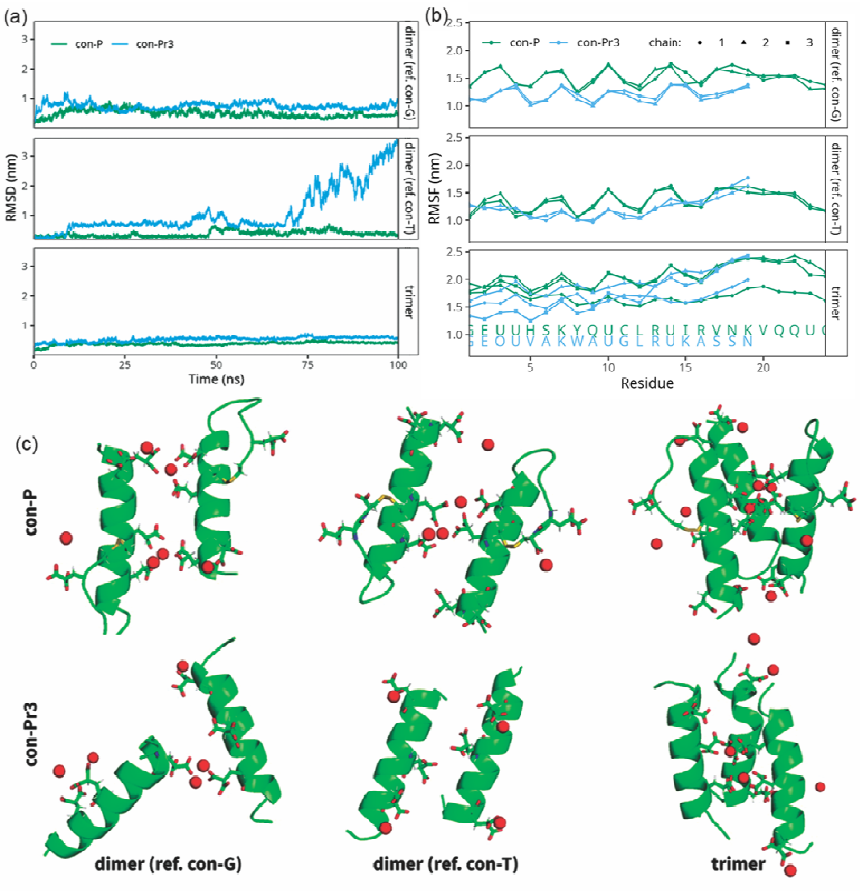

Fig. 6 — Simulations in the presence of Ca^{2+} show con-P and con-Pr3 can form stable metallozipper dimers and trimers. (a) Total protein RMSD of the complexes; (b) RMSF per-residue per chain; and (c) Most represented structures

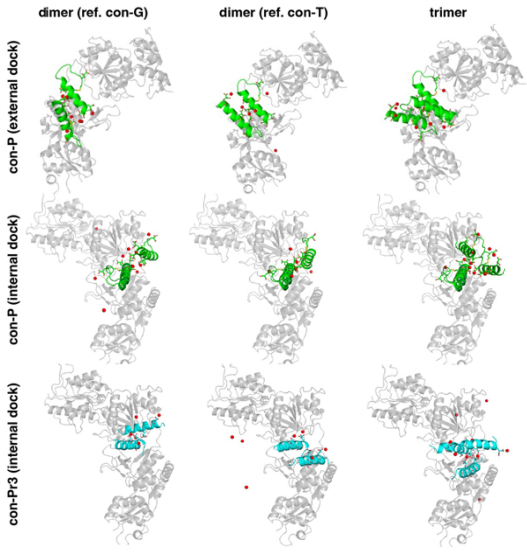

Fig. 7 — Aligned dimer and trimer assemblies of conantokins at GluN2B. The grid displays the structural organization of con-P (external/internal) and con-Pr3 (internal) in dimeric (ref. con-G, ref. con-T) and trimeric states. Red spheres indicate Ca^{2+}. Note the robust coordination and helical stability in con-P across all states, contrasted by the structural dissociation and sparse ion recruitment in con-Pr3 internal assemblies

Table 3 — Estimation of binding energy as MMPBSA between conantokins and GluN2B

Conantokin	Face on ATD-ABD Pocket	State	ΔG MMPBSA (kcal/mol)			
			Complex	Receptor	Ligand	Binding Energy
Con-P	External	Ca^{2+}-free	-8027.82	-6488.42	-1574.11	34.72
		Ca^{2+}-bound	-8106.37	-6566.32	-1558.30	18.25
	Internal	Ca^{2+}-free	8413.93	9937.78	-1583.43	59.58
		Ca^{2+}-bound	-7984.26	-6529.35	-1551.00	96.09
Con-Pr3	External	Ca^{2+}-free	-7543.58	-6712.33	-818.85	-12.40
		Ca^{2+}-bound	-7551.89	-6787.14	-803.80	39.05
	Internal	Ca^{2+}-free	-7443.97	-6635.43	-825.57	17.03
		Ca^{2+}-bound	-7428.61	-6622.61	-808.29	2.29

These results expand on the preliminary docking studies conducted by Waqar and Batool[25]. In their study, they computed binding energies of -15.45 kcal/mol for con-P and -10.20 kcal/mol for con-Pr3. Our results predict similar magnitudes of binding energy for con-Pr3, which were predicted to assume helical structures in both studies. In contrast, our study predicts lower binding affinities for con-P compared to con-Pr3. We attribute these differences to our inclusion of the disulfide bond (Cys11-Cys24), which resulted in a different modelled structure upon equilibration, prior to molecular docking. Additionally, this study suggests the significance of Ca^{2+} for the binding of the Gla-rich conantokins, particularly for the facilitation of residue contacts that promote functional binding interactions.

Conclusion

In the present work, it was determined that Ca^{2+} binding contributed to salt-bridge formation between GluN2B and the Gla residues of con-P and con-Pr3. These interactions were observed to influence con-P and con-Pr3 dimer and trimer stability. Ca^{2+} binding was also observed to influence the predicted binding affinities of con-P and con-Pr3 for target sites on GluN2B. These results provide structural bases for the preferential binding of these conantokins to their target NMDA receptor subunit. By acting as GluN2B antagonists, these conantokins can possibly prevent the deleterious effects of neuroexcitotoxicity caused by glutamate neurotransmitters and serve as foundations for novel therapeutic strategies.

Acknowledgement

We appreciate the support of the University of the Philippines Manila (ANPG), and the University of the Philippines Baguio (ECJ), the National Institute of Molecular Biology and Biotechnology, University of the Philippines Diliman (NADB, SKCA), and the UP-Philippine Genome Center – Protein, Proteomics and Metabolomics Facility, UP System (NADB, SKCA).

Conflict of interest

All authors declare no conflict of interest.

References

1 Cheriyan J, Balsara RD, Hansen KB & Castellino FJ, Pharmacology of triheteromeric N-methyl-d-aspartate receptors. *Neurosci Lett*, 617 (2016) 240.

2 Stroebel D, Casado M & Paoletti P, Triheteromeric NMDA receptors: from structure to synaptic physiology. *Curr Opin Physiol*, 2 (2018) 1.

3 Danysz W & Parsons CG, Alzheimer's disease, β-amyloid, glutamate, NMDA receptors and memantine – searching for the connections. *British J Pharmacol*, 167 (2012) 324.

4 Jimenez EC, Peptide antagonists of NMDA receptors: Structure-activity relationships for potential therapeutics. *Peptides*, 153 (2022) 170796.

5 Cnudde SE, Prorok M, Dai Q, Castellino FJ & Geiger JH, The crystal structures of the calcium-bound con-G and con-T[K7γ] dimeric peptides demonstrate a metal-dependent helix-forming motif, *J Am Chem Soc*, 129 (2007) 1586–93.

6 Prorok M, Warder SE, Blandl T & Castellino FJ, Calcium binding properties of synthetic γ-carboxyglutamic acid-containing marine cone snail "sleeper" peptides, conantokin-G and conantokin-T. *Biochemistry*, 35 (1996) 16528.

7 Cnudde SE, Prorok M, Jia X, Castellino FJ & Geiger JH, The crystal structure of the calcium-bound con-G[Q6A] peptide reveals a novel metal-dependent helical trimer. *J Biol Inorg Chem*, 16 (2011) 257.

8 Gowd KH, Twede V, Watkins M, Krishnan KS, Teichert RW, Bulaj G & Olivera BM. Conantokin-P, an unusual conantokin with a long disulfide loop. *Toxicon*, 52 (2008) 203.

9 Teichert RW, Jimenez EC, Twede V, Watkins M, Hollmann M, Bulaj G & Olivera BM, Novel conantokins from *Conus parius* venom are specific antagonists of N-Methyl-D-aspartate receptors. *J Biol Chem*, 282 (2007) 36905.

10 Zheng W, Zhang C, Li Y, Pearce R, Bell EW & Zhang Y, Folding non-homologous proteins by coupling deep-learning contact maps with I-TASSER assembly simulations. *Cell Rep Methods*, 1 (2021) 100014.

11 Jo S, Kim T, Iyer VG & Im W, CHARMM-GUI: A web-based graphical user interface for CHARMM. *J Comput Chem*, 29 (2008) 1859.

12 Roy A, Kucukural A & Zhang Y, I-TASSER: a unified platform for automated protein structure and function prediction. *Nat Protoc*, 4 (2010) 725.

13 Zhang JB, Chang S, Xu P, Miao M, Wu H, Zhang Y, Zhang T, Wang H, Zhang J, Xie C, Song N, Luo C, Zhang X & Zhu S, Structural basis of the proton sensitivity of human GluN1-GluN2A NMDA receptors. *Cell Rep*, 25 (2018) 3582.

14 Schrödinger L, (2010) The PyMOL Molecular Graphics System, Version 1.3r1.

15 Bekker H, Berendsen H, Dijkstra E, Achterop S, Vondrumen R, Vanderspoel D, Sijbers A, Keegstra H & Renardus M, GROMACS - a parallel computer for molecular-dynamics simulations, In: *Physics Computing '92*, (Ed. by R DeGroot & J Nadrchal), 1993, 252.

16 Croitoru A, Park SJ, Kumar A, Lee J, Im W, MacKerell AD Jr & Aleksandrov A, Additive CHARMM36 force field for nonstandard amino acids. *J Chem Theory Comput*, 17 (2021) 3554

17 Humphrey W, Dalke A & Schulten K, VMD: Visual molecular dynamics. *J Mol Graph*, 14 (1996) 33.

18 Amadei A, Linssen ABM & Berendsen HJC, Essential dynamics of proteins. *Proteins*, 17 (1993) 412.

19 Kozakov D, Hall DR, Xia B, Porter KA, Padhorny D, Yueh C, Beglov D & Vajda S, The ClusPro web server for protein–protein docking. *Nat Protoc*, 12 (2017) 255.

20 Valdés-Tresanco MS, Valdés-Tresanco ME, Valiente PA & Moreno E, gmx_MMPBSA: A new tool to perform end-state free energy calculations with GROMACS. *J Chem Theory Comput*, 17 (2021) 6281.

21 Kaiser TM, Kell SA, Kusumoto H, Shaulsky G, Bhattacharya S, Epplin MP, Strong KL, Miller EJ, Cox BD, Menaldino DS, Liotta DC, Traynelis SF & Burger PB, The bioactive protein-ligand conformation of GluN2C-selective positive allosteric modulators bound to the NMDA receptor. *Mol Pharmacol*, 93 (2018) 141.

22 Khatri A, Burger PB, Swanger SA, Hansen KB, Zimmerman S, Karakas E, Liotta DC, Furukawa H, Snyder JP & Traynelis SF, Structural determinants and mechanism of action of a GluN2C-selective NMDA receptor positive allosteric modulator. *Mol Pharmacol*, 86 (2014) 548.

23 Zhu S, Stein RA, Yoshioka C, Lee CH, Goehring A, Mchaourab HS & Gouaux E, Mechanism of NMDA receptor inhibition and activation. *Cell*, 165 (2016) 704.

24 Tian M, Stroebel D, Piot L, David M, Ye S, & Paoletti P, GluN2A and GluN2B NMDA receptors use distinct allosteric routes. *Nat Commun*, 12 (2021) 4709

25 Waqar M & Batool S, *In silico* analysis of binding interaction of conantokins with NMDA receptors for potential therapeutic use in Alzheimer's disease. *J Venom Anim Toxins Incl Trop Dis* 23 (2017) 42.

26 McIntosh JM, Olivera BM, Cruz LJ & Gray WR, Gamma-carboxyglutamate in a neuroactive toxin. *J Biol Chem*, 259 (1984) 14343.

27 Donevan SD & McCabe RT, Conantokin G is an NR2B-selective competitive antagonist of *N*-methyl-d-aspartate receptors. *Mol Pharmacol*, 58 (2000) 614.

28 Haack JA, Rivier J, Parks TN, Mena EE, Cruz LJ & Olivera BM, Conantokin-T. A gamma-carboxyglutamate containing peptide with N-methyl-d-aspartate antagonist activity. *J Biol. Chem*, 265 (1990) 6025.

29 Huang L, Balsara RD & Castellino FJ, Synthetic conantokin peptides potently inhibit N-methyl-D-aspartate receptor-mediated currents of retinal ganglion cells. *J Neurosci Res*, 92 (2014) 1767.

30 White HS, McCabe RT, Armstrong H, Donevan SD, Cruz LJ, Abogadie FC, Torres J, Rivier JE, Paarmann I, Hollmann M & Olivera BM, *In vitro* and *in vivo* characterization of conantokin-R, a selective NMDA receptor antagonist isolated from the venom of the fish-hunting snail *Conus radiatus*. *J Pharmacol Exp Ther*, 292 (2000) 425

31 Twede VD, Teichert RW, Walker CS, Gruszczyński P, Kaźmierkiewicz R, Bulaj G & Olivera BM, Conantokin-Br from *Conus brettinghami* and selectivity determinants for the NR2D subunit of the NMDA receptor. *Biochemistry*, 48 (2009) 4063.

32 Gowd KH, Han TS, Twede V, Gajewiak J, Smith MD, Watkins M, Platt RJ, Toledo G, White HS, Olivera BM & Bulaj G, Conantokins derived from the *Asprella* clade impart con *Rl* -B, an N-methyl D-aspartate receptor antagonist with a unique selectivity profile for NR2B subunits. *Biochemistry*, 51 (2012) 4685.

33 Platt RJ, Curtice KJ, Twede VD, Watkins M, Gruszczyński P, Bulaj G, Horvath MP & Olivera BM, From molecular phylogeny towards differentiating pharmacology for NMDA receptor subtypes. *Toxicon*, 81 (2014) 67.